Polymer 51 (2010) 6005–6012

Contents lists available at ScienceDirect

Polymer

journal homepage: www.elsevier.com/locate/polymer

Structural properties and superhydrophobicity of electrospun polypropylene fibers from solution and melt

Daehwan Cho [a], Huajun Zhou [a,b], Youngjin Cho [b], Debra Audus [a], Yong Lak Joo [a,*]

[a] School of Chemical and Biomolecular Engineering, Cornell University, Ithaca, NY 14853, United States
[b] Department of Materials Science & Engineering, Cornell University, Ithaca, NY 14853, United States

ARTICLE INFO

Article history:
Received 22 July 2010
Received in revised form
8 October 2010
Accepted 12 October 2010
Available online 20 October 2010

Keywords:
Electrospinning
Polypropylene
Hydrophobicity

ABSTRACT

Isotactic polypropylene (iPP) has successfully been electrospun from both solution and melt using an elevated temperature setup. First, PP nanofibers with two different average diameters (0.8 μm and 9.6 μm) were obtained via electrospinning of iPP in decalin, and the effect of deformation and solidification on the morphological and structural features of the resulting fibers was studied. Secondly, melt electrospun PP fibers with two different average diameters were also fabricated to compare the structures with those of solution electrospun PP fibers. DSC and XRD results show that β form crystals which can increase the impact strength and toughness of electrospun fibers are present in sub-micron scale PP fibers from solution, while fibers from melt mostly show α form crystals. The annealed fibers have changed their morphological forms into α and γ crystal forms. Finally, it is observed that electrospun PP fiber webs both from solution and melt exhibit superhydrophobicity with a water contact angle about 151° which is substantially higher than those of a commercial PP non-woven web and a compression molded PP film, 104° and 112°, respectively. Such superior hydrophobicity was observed for all PP electrospun fibers and it was not altered by the processing scheme (solution or melt) or fiber diameter (sub-micron or micron). Enhanced hydrophobicity of electrospun PP fiber webs contribute to excellent barrier performance without losing permeability when they are applied to protective clothing.

1. Introduction

Polypropylene (PP) fiber is one of the lightest synthetic fibers available and comprises the majority of non-woven polyolefin fibers which are of great commercial interest due to their unique properties which include hydrophobicity, good mechanical strength, and excellent chemical resistance [1]. In recent years, sub-micron polyolefin fibers are sought to meet the demands in the fields of filtration, battery separators and protective coating because of their enhanced high surface area to mass ratio [2–4].

Electrospinning has been widely studied during the past few years, which many polymers have been reported to be successfully electrospun [5–13]. The mechanism of jet thinning [7,8,12] and the effects of a variety of parameters [5,10,13] on electrospinning have been investigated to provide a better understanding of the electrospinning process. However, electrospinning of polyolefin is still in early stages and only few studies have been published mainly because electrospinning of polyolefin requires either melting it directly or dissolving it into a solvent at elevated temperature. Larrondo et al. was the first to report on applying an electrical field to polyolefin melts to obtain their fiber form, but the instabilities that cause thinning of the jet via the whipping motion had not been fully explored, leading to the collection of thick fibers (~ 50 μm) [14–16]. Lyons and co-workers systematically studied the effect of processing conditions on electrospinning PP fibers from its melt and found that molecular weight was the most important factor in obtaining thin fibers [17,18]. Average fiber diameters of PP fibers from melt electrospinning in their study were well above micron. Recently, we have reported that the vigorous whipping motion can be achieved even in melt electrospinning if spinning temperature is kept high enough to prevent premature solidification of the melt jet, and thus the thermal effect such as spinning temperature is very important in producing sub-micron sized polylactic acid fibers from the melt [19]. More recently, melt electrospinning has been applied to nylon 6 and melt electrospun fibers with slightly less than micron in diameter have been obtained [20]. We extend our melt electrospinning approach to heated solution electrospinning of polyolefin in the current study to obtain sub-micron sized polyolefin fibers. For the PP fiber webs from solution and melt, we compare their structural properties including degree of crystallinity

* Corresponding author. Tel.: +1 607 255 8591; fax: +1 607 255 9166.
E-mail address: ylj2@cornell.edu (Y.L. Joo).

0032-3861/$ – see front matter © 2010 Elsevier Ltd. All rights reserved.
doi:10.1016/j.polymer.2010.10.028

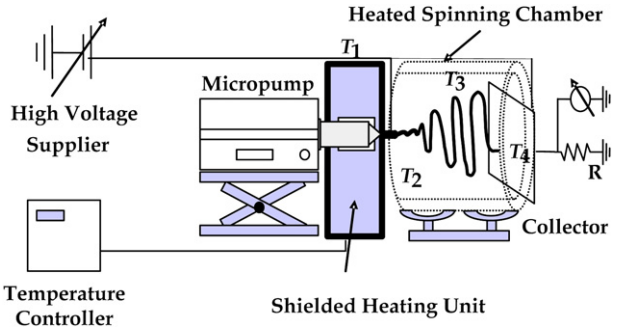

Fig. 1. Schematic diagram of an electrospinning setup used in the current study.

and types of crystal forms that may influence the material properties of PP fibers.

Recently, exploring the possibility of producing superhydrophobic fiber webs through electrospinning has been intensively carried out [21–23]. Researchers in the Rutledge group studied the superhydrophobicity of poly(styrene-*block*-dimethylsiloxane) block copolymer fibers and concluded that it is attributed to the combined effects of surface enrichment of siloxane and the surface roughness of the fiber web [22]. Other researchers such as Singh and co-workers synthesized a novel fluoro-polymer that exhibits low surface energy to obtain superhydrophobic film via electrospinning [23]. The wettability of a film depends on the surface energy and surface roughness according to the theory of roughness-induced hydrophobicity developed by Wenzel and Cassie-Baxter [24,25]. Superhydrophobicity can be produced by generating sub-micron or micron scale roughness on the inherently hydrophobic surface [26]. Electrospinning can exactly replicate a desired roughness at this length scale and thus can be a promising scheme to introduce superhydrophobicity to various materials. Combined methods of electrospinning and coating of hydrophobic materials are also reported in several papers. Ma et al. combined the methods of electrospinning and initiated chemical vapor deposition to produce superhydrophobic poly(caprolactone) surface coated with hydrophobic polymerized perfluoroalkyl ethyl methacrylate [27]. In their work electrospinning was utilized to generate a sub-micron scale roughness and coating of the hydrophobic materials enables the superhydrophobicity. Electrospinning of PP which is inherently hydrophobic can offer a more straightforward, single-step approach to produce superhydrophobicity compared to the methods described above which involves either complicated synthesis of hydrophobic materials or additional coating.

In the current study, we successfully set up an experimental device to carry out electrospinning of PP directly from melt or heated solution at elevated temperature. The effects of spinning parameters through the solution electrospinning, especially with nozzle temperature and spinning temperature, on fiber morphology are investigated. The resulting fiber webs from both solution and melt electrospinning processes are characterized thoroughly, and the morphology, thermal properties, structural characteristics and superhydrophobicity of electrospun PP fibers are presented. Barrier performance of pesticide penetration is analyzed to evaluate the feasibility of PP electrospun fiber webs as a protective coating.

2. Experimental section

2.1. Electrospinning processes from solution at elevated temperature and melt

This study employed the PP chips which had a molecular weight of 129,000 and polydispersity of 2.8 from Clarcor. We prepared a concentrated solution of 10 wt% of PP in Decalin with 0.5 wt% of antioxidant at 130 °C for the solution electrospinning. The experimental setup shown in Fig. 1 was employed in our electrospinning experiments at elevated temperature. This setup was designed to have a precise, independent control of the temperatures of solution or melt reservoir, nozzle and spinning region. It consists of four temperature zones: solution reservoir (T_1), nozzle (T_2), spinning region (T_3) and collector (T_4). All these temperatures are demonstrated to be important to control either fiber morphology or fiber structure. Among them, nozzle temperature is crucial to the success of obtaining sub-micron size fibers [6]. For the solution electrospinning, PP solution is kept in a reservoir at relatively low temperature enough to maintain the solution, while nozzle temperature is adjusted to obtain the optimal spinning viscosity. The temperature of a spinning region controls the solidification of the jet through balancing solvent evaporation and gelation of the jet. The control of a collector temperature is a great addition to regulate the crystallinity of fibers in line by annealing or quenching. The PP in decalin solution was loaded into a 5 mL syringe with an 18 gauge needle and mounted in the solution spinning setup which had been preheated with $T_1 = 130$ °C, $T_2 = 155$ °C, $T_3 = 95$ °C. Flow rate was set at 0.02 ml/min. T_2 was varied from 140 °C to 170 °C to study the effect of nozzle temperature. It is worth noting that the needle was connected to a positive power supply and the collector to a negative power supply (Gamma High Voltage) instead of ground in normal cases. The voltage on the needle is noted as $V+$ and collector as $V-$. $V+$ was set from 3 kV to 8 kV and $V-$ at −12 kV with the collecting distance at 3 inches. Fibers were collected onto an aluminum plate.

In case of a melt electrospinning, PP pallets were filled into a 5 mL syringe with a 30 gauge needle and the temperature of all four of the aforementioned zones was controlled by setting the temperature at T_1 = 240 °C, T_2 = 180 °C for the fibers with a diameter 2.4 μm or T_2 = room temperature for the fibers with 8.5 μm, T_3 = room temperature. The flow rate was set at 0.001 ml/min. An electrical charge of 28 kV was set to the collector using a positive power supplier and −5 kV at the needle. The distance between a collector and a needle was set 2 inches which were shorter than one of solution.

2.2. Morphology and structure characterizations

As-spun fibers were then subjected to various characterizations. Electrospun fiber diameter and surface morphology were determined by a scanning electron microscopy (Leica 440). A Capillary Flow Porometer (Porous Materials, Inc, Ithaca, NY) measured pore size distribution of sample webs. Four drops of SilWick fluid were used as a wetting agent. The porometer works by increasing gas pressure through wet and dry samples to measure the pore

Table 1
Preparation of mixture solutions with different pesticides and surface tensions.

Mixture code	Pesticide	Mixture solution			Surface tension (dynes/cm)
		Water (g)	Pesticide (g)	Oil (g)	
P1	Atrazine 90WDG	245	2.5	–	38.0
P2	Prowl 3.3 EC	55	23.3	14	31.0

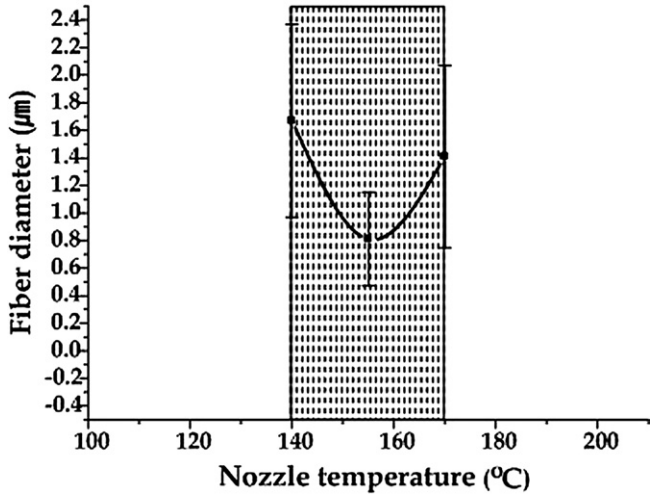

Fig. 2. Effect of nozzle temperature on the average diameter of electrospun PP fibers from 10 wt% of PP in decalin solution.

diameters of through-pores. Thermal properties were analyzed by differential scanning calorimetry (Seiko, DSC 220C) with heating rate at 10 °C/min in nitrogen atmosphere until the temperature reached 200 °C. Structural studies were performed through XRD (Scintag, Inc. Theta–Theta Diffractometer) in the 2θ range of 5–35°, in steps of 0.02° and a scanning rate of 3° per minute. Water contact angle was measured through a Contact Angle Analyzer manufactured by Imass, Inc.

2.3. Protection performance

Three variables related to protection performance were achieved by each Standard Test Method. Air permeability of each web was measured by ASTM D 737-96. Water vapor transmission rate was measured according to ASTM E 96-00. ASTM F 2130-01 was adopted to assess pesticide repellency and penetration (all procedures are well described in the reference [3]). In Table 1, the pesticide concentration and surface tension are shown to prepare the mixture solutions for the pesticide penetration test. The mixture P2 is designed to lower surface tension in order to compare the penetration results of pesticide with the hydrophobic ones measured by a mixture droplet of water and ethanol.

For the protein adsorption test, 0.5 mg of bovine serum albumin (BSA) labeled with fluorescein isothiocyanate (BSA-FITC) was dissolved in 5 mL of PBS buffer solution. PP non-woven webs and PP electrospun SF fiber webs were prepared to measure the protein adsorption on the fiber surface. The three fiber surfaces were then incubated in BSA-FITC solution in a dark room for 2 h and rinsed with PBS buffer solution and deionized water thoroughly afterwards. Fluorescence microscopy was performed using an Olympus BX51 upright microscope with a 40x UPlan Fluorite 40× dry objective (N.A. 0.75). Images were acquired using a Roper Cool Snap HQ CCD camera and Image Pro image acquisition and processing software. Fluorescein and FITC were observed with a 450 nm excitation and 550 nm emission filter set.

Table 2
Average fiber diameter and processing conditions and methods employed in the study.

Sample code	Fiber diameter (μm)		Temperature at collector	Spinning method
	avg[1]	std		
S1	0.8	0.25	40	Heated solution
S2	0.8	0.25	120	Heated solution
S3	9.6	3.4	120	Heated solution
M1	2.4	0.4	40	Melt
M2	2.4	0.4	120	Melt
M3	8.5	1.4	120	Melt

[1] avg: average of 30 fibers, std: standard deviaton of 30 fibers.

3. Results and discussion

3.1. Processing conditions and morphology

As discussed in other literatures [5,8,10], processing parameters such as solution concentration, flow rate, spinning voltage, spinning temperature and collecting distance are all important factors to affect the morphology of electrospun non-woven fiber webs. We found that the temperature of a needle and a spinning zone would be critical to the success of electrospinning as in melt electrospinning of PLA [19], In case of polyolefin solution electrospinning at elevated temperature, nozzle temperature is set to an optimal value between solution gelling temperature and solvent boiling temperature. For 10 wt% concentration of PP in decalin solution, a successful electrospinning for continuous production of fibers was not achieved with T_2 below 140 °C or above 170 °C because of either fast gelling or fast solvent evaporation. Fig. 2 shows the operable window of nozzle temperature and its effect on the average diameter of PP fibers collected at the same conditions. To obtain sub-micron scale fibers, 155 °C was found to be the optimum nozzle temperature. At this temperature, the smallest fibers with small variation were produced. Otherwise the thicker fibers were obtained from high concentration (25 wt%) of PP in decalin, which the smooth fibers with relatively large diameter (9.6 μm) would be electrospun. The solution concentration not only affects the viscosity of the solution but also controls indirectly the evaporation of the solvent since decalin has a high boiling point at 176 °C.

Electric conductivity is a key parameter in determining the charge density of the solutions, and is closely related to the stretching force during electrospinning. Polyolefin in decalin solution has an extremely low conductivity compared to other typical polar solutions, which makes the initiation of electrospinning

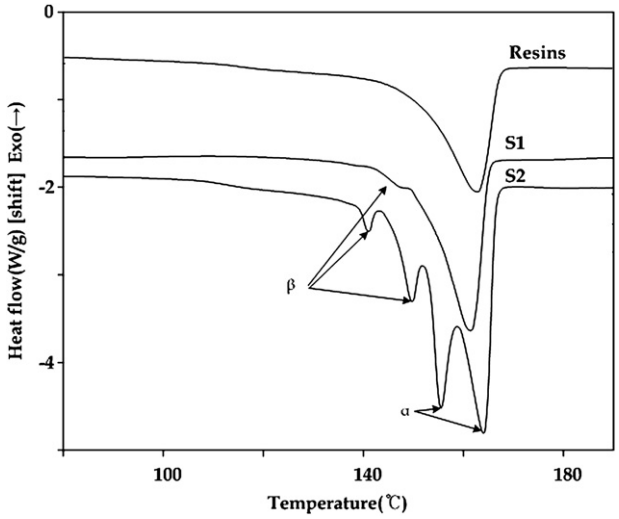

Fig. 3. DSC curves of PP resins and PP fibers collected at 40 °C (S1 fiber) and 120 °C (S2 fiber) during solution electrospinning.

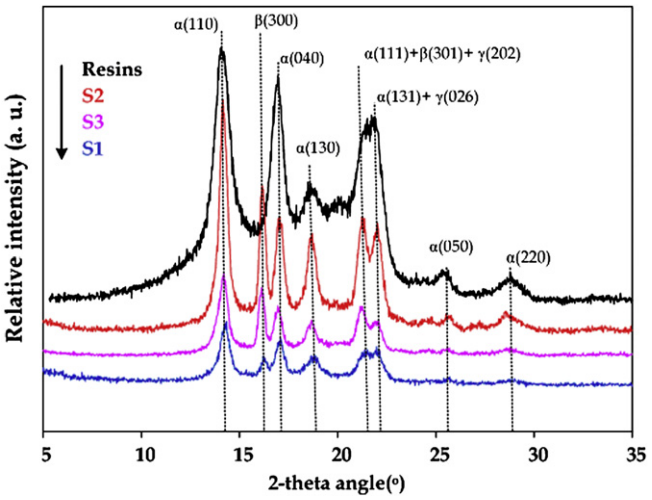

Fig. 4. XRD reflection patterns for PP resins, sub-μm PP fibers acquired at 40 °C (S1 fiber) and 120 °C (S2 fiber) and ones with 9.6 μm prepared at 120 °C (S3 fiber).

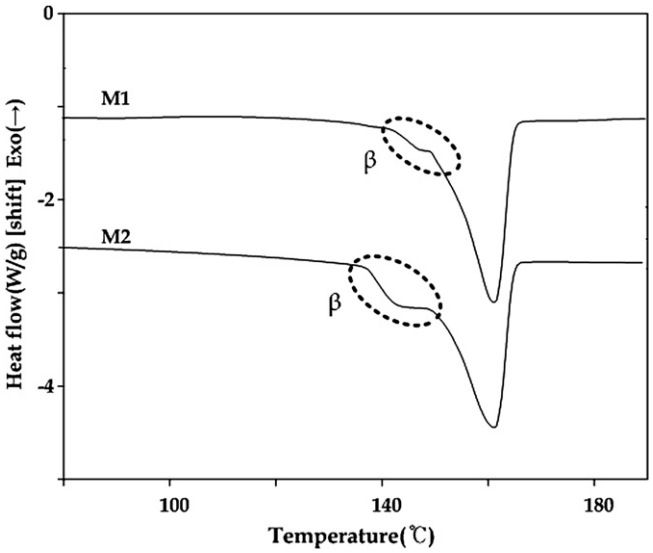

Fig. 5. DSC curves of PP fibers collected at 40 °C (M1 fiber) and 120 °C (M2 fiber) during melt electrospinning.

difficult. The combination of positive polarity on the needle and negative polarity on the collector helps the jet eject out of the needle and experience greater stretching force. For the melt spinning in the study, we also controlled the temperature of needle and spinning zone. With the same temperature of needle (T_1), we could obtain the fibers with a fine diameter of 2.4 μm when the temperature of spinning zone (T_2) was increased to the 180 °C; whereas the fibers with 8.5 μm diameter would be obtained without heating the spinning zone. As shown in Table 2, all the samples are summarized to be prepared in this paper.

3.2. Thermal properties and crystal structures

PP has three types of crystal structures: α, β and γ crystal forms [26]. The most common crystal form in PP is the α crystals that are thermodynamically the most stable phase having a monoclinic crystal structure and the primary form under normal processing conditions. The β crystals are usually observed in the presence of nucleating sites or under a strong imposed orientation. PP with the β crystals exhibits better impact strength and toughness than in α crystal. The γ crystals can be formed during crystallization under high pressure (above 200 MPa) and rather similar to the situation of lamellar branching in the α crystals that can act as a nucleus for the γ crystals. It has been reported that electrospun fibers exhibit to some extent meta-stable phases possibly due to two reasons: deformation of the jet and fast solidification (fast solvent evaporation or/and rapid temperature drop) [6,28]. Elongation deformation in electrospinning processes tends to align polymer molecules, and subsequent rapid solidification can freeze the alignment of molecules.

The DSC curves for two fibers with a sub-micron diameter from solution and as-received PP resin are shown in Fig. 3. Sub-micron sized PP fibers obtained from solution electrospinning exhibit meta-stable β crystals, whereas for the PP resin, there is only one endothermic peak around 162.5 °C which is the melting peak for the α crystal phase. To investigate the effect of in situ annealing/recrystallization at the collector, one fiber was collected with the collector temperature (T_4) at 40 °C (denoted as S1 fiber) and the other was collected at 120 °C (S2 fiber), while keeping all other conditions the same. As shown in Fig. 3, for S1 fiber, there is a small shoulder with the main endothermic peak at lower temperature around 146.9 °C. The curve for S2 fiber has four distinct peaks, where two of them represent the α melting peaks and the other two represent β melting ones. This peak splitting is closely associated with a degree of perfection of the crystals. S1 fiber was collected at the temperature where PP crystallizes much slowly, whereas S2 fiber fibers may have enough thermal energy to recrystallize at 120 °C which can cause the splitting [28,29]. The heat of fusion for pure PP is taken as 188 J/g. The degree of crystallinity based on this value for S1 fiber of whose fusing heat is 99.6 J/g is 53.0%. The crystallinity of S2 fiber (fusing heat: 111.7 J/g) on the other hand shows 59.4% assuming that the heats of fusion

Table 3
Degree of crystallinity and β content of PP resins and fibers.

Items	Crystallinity (%)	k_β (%)	Remark
PP resins	32.0	0	PP resins
S1	53.6	8.1	Electrospun fibers
S2	65.0	26.9	from heated solution
S3	63.4	19.0	
M1	43.5	0	Electrospun
M2	54.3	25.8	fibers from melt
M3	51.4	14.8	

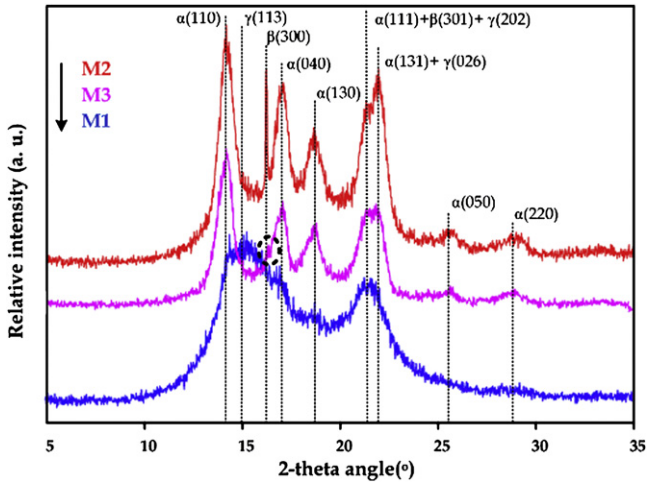

Fig. 6. XRD reflection patterns for thin and thick PP fibers acquired at 120 °C (M2 fiber, M3 fiber, respectively) and one PP fiber with a 2.4 μm prepared at 40 °C (M1 fiber).

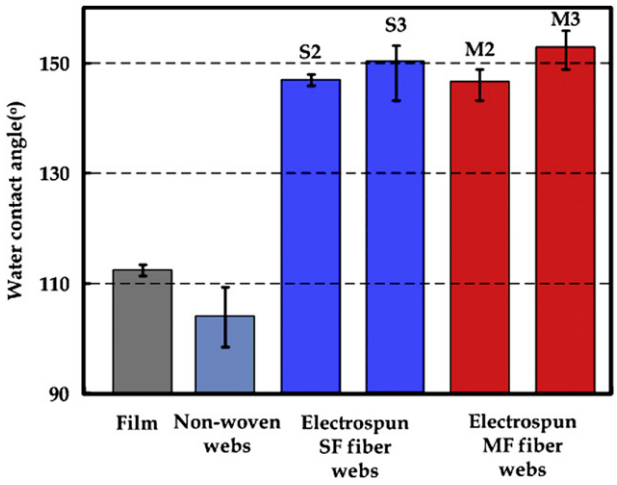

Fig. 7. Water contact angles of six different PP surfaces: compression molded PP film, PP non-woven webs, and four electrospun webs from solution and melt (error bar represents maximum and minimum angles during measurement of three times).

for the α and the β are the same. The part of the deformed structures are frozen in the fibers at 40 °C, whereas the S2 fiber with the high collecting temperature enables PP molecules with more energy to recrystallize, and thus increases the total degree of crystallinity of as-spun fibers.

The structural changes of PP fibers are further confirmed by the XRD studies in which we investigate not only the relationship between fiber diameter and β content but also differences between the fibers obtained at different collector temperatures. The most distinct change for fibers is found at the β (300) peak at around 16.2° in Fig. 4. After the deconvolution of the XRD curves, we can obtain the detailed phase composition in each fiber system. The β content is estimated based on the calculation of the Turner Jones parameter, k_β, given by a reference [30].

$$k_\beta = I_{\beta(300)} / \left(I_{\beta(300)} + I_{\alpha(110)} + I_{\alpha(040)} + I_{\alpha(130)} \right) \quad (1)$$

According to the Table 3 in which the crystallinity data were measured by the XRD reflection, S2 fiber exhibits a higher degree of crystallinity (65.0%) than S1 fiber (53.6%) which agrees with our DSC study. The degree of β content is also larger for S2 fiber (26.9%) than that for S1 fiber (8.1%). This suggests that the frozen elongated structures crystallize into β crystals at 120 °C, which is relatively stable at this temperature, and thus no significant transformation from β to α crystals takes place. However, at 40 °C, the highly elongated chains remain as amorphous structures.

To confirm the assumption that the β content is also associated with degree of deformation, a fiber sample with an average diameter of 9.6 microns from solution (S3 fiber) were collected at 120 °C with the same conditions. These thick fibers are understood to experience a lower degree of elongational deformation. It has a slightly lower crystallinity (63.4%) compared to S2 fiber (65.0%), while the β composition is significantly smaller than S2 fiber (19.0% vs. 26.9%). This result suggests that the formation of the β crystals is favored by the strong deformation and high annealing temperature. To compare the morphological features of the fibers from melt electrospinning with those from solution, melt electrospun fibers with 2.4 μm diameter were deposited at the collect. It should be noted that according to our recent comparison of online temperature measurement during electrospinning to non-isothermal simulation for various polymers including PP [31], enhanced heat transfer caused by electrohydrodynamically driven air flow near the jet lead to rapid quenching of the melt jet.

Such quenching was more substantial for the non-conducting polypropylene jet due to the stronger electrohydrodynamic effect, and thus obtaining thin PP fibers from melt electrospinning was much more difficult. Producing sub-micron scale PP fibers with a modified melt electrospinning setup which ensures high melt jet temperature is currently underway [32]. In Fig. 5, the DSC curves for melt electrospun fibers with a 2.4 μm diameter at the collector at $T_4 = 40$ °C (M1 fiber) and at $T_4 = 120$ °C (M2 fiber) are shown. The PP fibers (M2 fiber) show a big dent with the curve at the temperature around 140 °C that is regarded as a crystallization region at the meta-stable β crystals. Unlike that of solution electrospun PP fibers, the DSC curve of the melt electrospun fibers (M2 fiber) does not show distinct double melting peaks. It may suggest

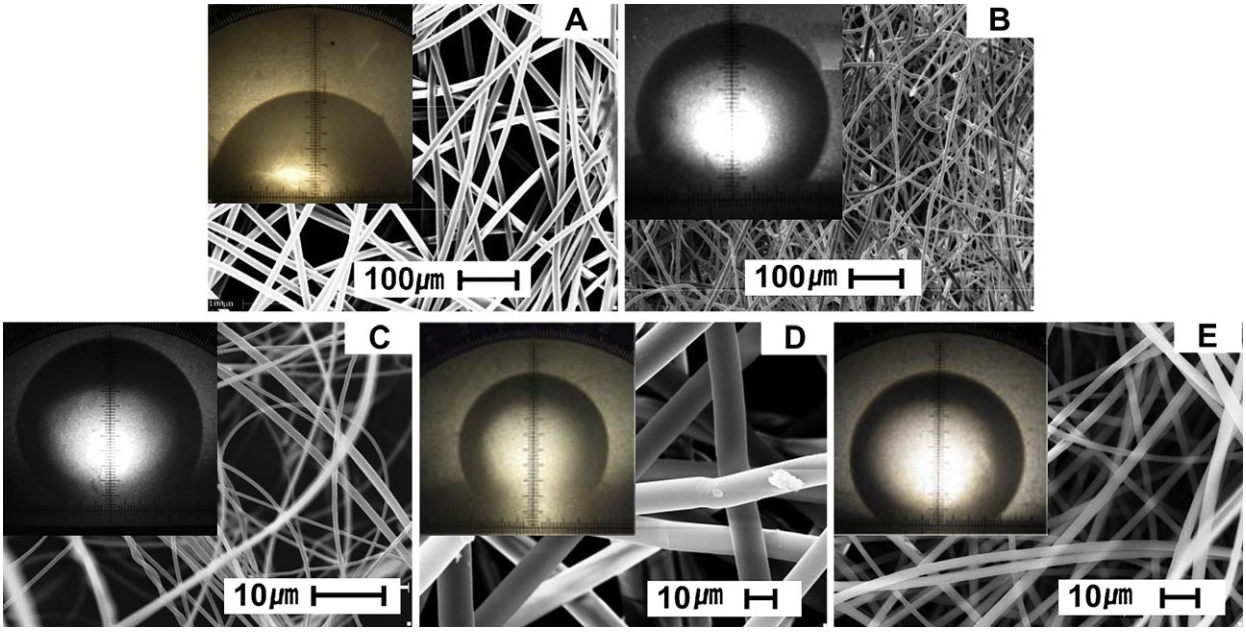

Fig. 8. SEM images of the web samples and water droplets on them; Non-woven webs (A), electrospun webs of S3 (B), S2 (C), M3 (D), and M2 (E).

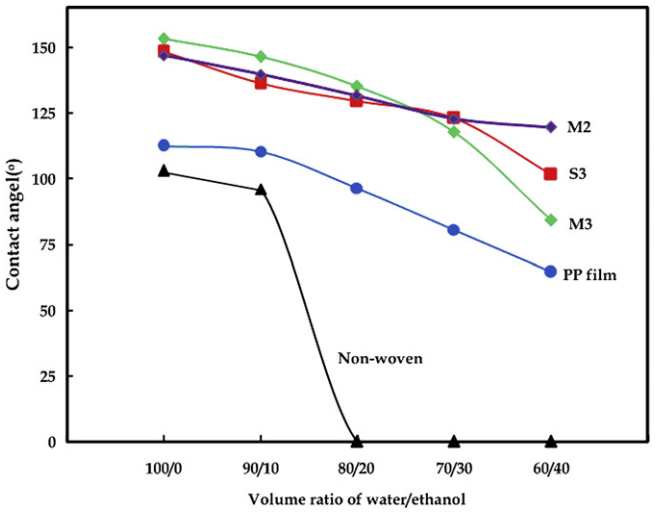

Fig. 9. Results of contact angle with electrospun fiber webs (S3, M2, M3), PP film, and non-woven webs according to the different droplet solutions.

that it is not easy to make an oriented crystal into the chain of fibers due to the higher viscosity and lower mobility associated with rapid quenching in melt electrospinning. The crystallinity calculated by the heat data of fusing pure PP, 188 J/g is 44.4% for M1 fiber (fusing heat: 83.5 J/g) and 49.2% for M2 fiber (fusing heat: 92.5 J/g), which are much lower than those from the solution.

The XRD patterns for melt electrospun fibers are shown in Fig. 6 and the degree of crystallinity and fraction of β crystals are listed in Table 3. It is observed that the fibers (M1 fiber) electrospun from the melt have α and γ crystals, but do not have a peak of β crystals. Even though a slight dent corresponding β crystals of M1 fiber is shown in DSC curve, all intensities over azimuthal angle are integrated in XRD patterns so that a slight signal like the β crystals of M1 fiber in DSC is difficult to be detected [33]. In case of thermally treated fibers (M2 fiber), the original crystal phases deform into several crystal phases due to heat treatment. The M3 fiber shows up small amount of peak of the β crystals, whereas the M2 fiber has a striking sharp peak at around 16.2° for the β crystals. This suggests that the M2 fiber with a fine diameter 2.4 μm from the melt electrospinning has been experienced higher degree of extension during spinning than the fiber with a thick diameter. The M2 fiber fibers contain a higher crystallinity than M1 fiber which well agrees with our DSC results. This trend of higher crystallinity and β content at the higher collection temperature in melt electrospun fibers is the same as that in solution electrospun fibers. However, the β contents and the percentage of crystallinity in the fibers from solution exhibit higher than those in the fibers from melt, which also corresponds to the results of DSC.

With the comparison between the fibers from solution and melt, we conclude that thin fibers by the larger degree of elongational deformation and high collection temperature favor the formation of β crystals. We also note that while the fibers from the solution spinning experienced the same trend of the increased β content with increasing deformation as those from the melt, low viscosity and slow evaporation of decalin in solution electrospinning lead to higher degree of crystallinity and enhanced the formation of β crystals than quenched fibers during melt electrospinning.

3.3. Hydrophobicity

As mentioned in the Introduction, the electrospinning using an inherently hydrophobic PP resins may result in superhydrophobicity of the as-spun fibers. In the present study, the water

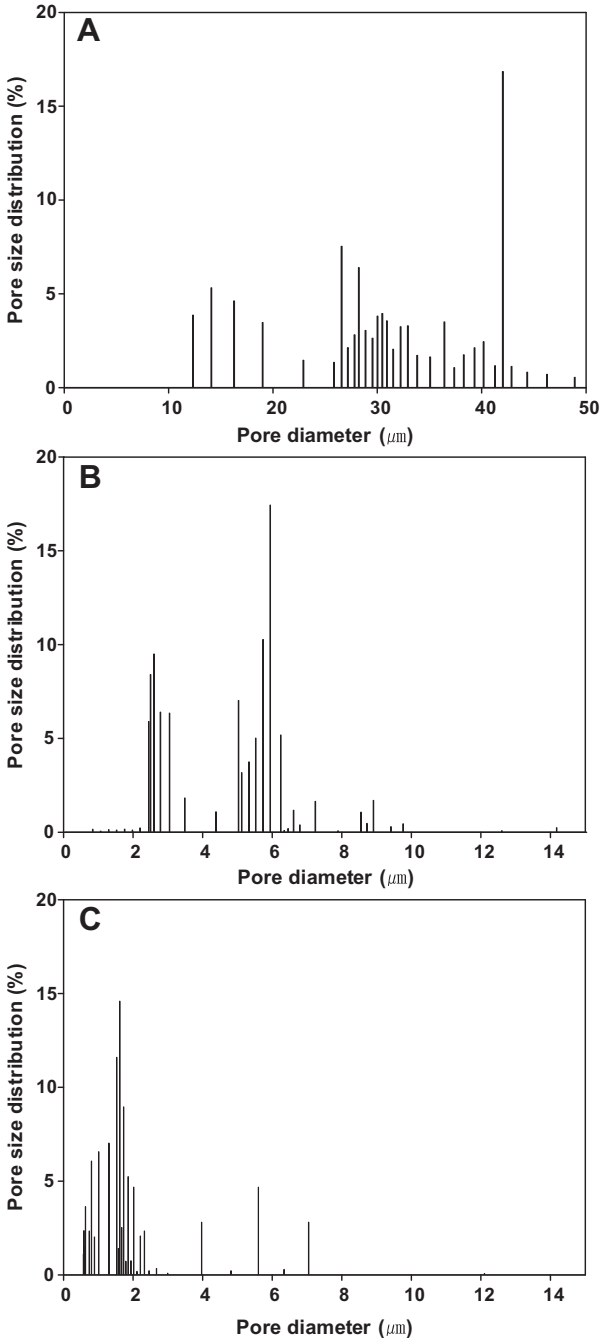

Fig. 10. Pore size distribution of PP non-woven substrate (A) and PP non-woven substrate covered with M3 electrospun fiber webs (B), and with S2 electrospun fiber webs (C).

contact angle of six samples are measured: a compression molded PP film, PP non-woven webs, two electrospun webs constituted fibers with a thick diameter from solution and melt, and two ones with fine scale diameter (sub-micron scale from solution and 2.4 μm scale from melt). The PP non-woven webs were obtained from DuPont, which were made by a melt blown process. The diameter of the fibers on the webs is around 15 μm and the porosity of the webs shows very large compared to the electrospun fiber webs. As shown in Fig. 7, the smooth PP film surface presents a water contact angle of 110° and PP non-woven web exhibits even lower angle 104° than the film. It is observed that the degree of hydrophobicity is significantly enhanced in the electrospun PP fiber

Table 4
Results of air permeability, water vapor transmission, and liquid repellency, penetration of PP non-woven substrate webs and substrate webs spun with melt (M3) and solution (S2).

Sample	Air permeability ($cm^3/s/cm^2$)	Water vapor transmission rate ($g/h/m^2$)	Mixture P1		Mixture P2	
			Repellency (%)	Penetration (%)	Repellency (%)	Penetration (%)
PP non-woven substrate webs	270	22.1	30	9	3	83
Substrate webs spun by melt (M3)	168	20.5	68	0	57.5	11
Substrate webs spun by solution (S2)	156	19.8	63	0	56	9

webs, which all webs with the electrospun fibers exhibit superhydrophobicity. The webs of thin fibers from melt have the water contact angle of 147° and the other webs of thicker fibers from melt had contact angle of 150°. The sub-micron scale fibers from solution even exhibit the water contact angle of 151° and the other ones from solution had 148°. The morphologies of webs and the water drops on their surface are shown in Fig. 8. According to the results of the contact angles with the four samples, there is only a slight difference between the fiber webs with different diameters. This suggests that the fiber diameter under 10 μm is sufficient to provide surface roughness for superhydrophobicity of PP fiber webs via electrospinning. We also note that the contact angles between fibers from melt and solution show no difference. The roughness measurement of the webs is unavailable through AFM because of the high porosities of the web surface. More rigorous studies on the contact angle with the hydro-properties of the hydrophilic and hydrophobic materials by analyzing the parameters to affect the contact angle such as porosity and diameter of the electrospun fibers is currently underway.

To elaborate the difference of hydrophobicity with various samples using a different solvent system, the mixture solutions were used to drop a droplet during the contact angle measurement. Five different solutions were prepared with a mixture of a specific volume ratio of water to ethanol such as 100:0, 90:10, 80:20, 70:30, and 60:40, respectively. It is interesting to note that as increasing the ratio of ethanol the contact angles gradually decreased with the electrospun fibers and PP film and showed larger difference among the electrospun fiber webs at a mixture 60:40.

In Fig. 9, the trend of contact angles between two fibers of M2 and M3 is inversely changed from the ratio of 70/30 and M2 sample shows higher contact angle as increasing the ratio of ethanol. Otherwise, the contact angle of non-woven webs is drastically dropped at the ratio of 80/20. As shown in Fig. 8, the non-woven webs show large porosity compared to other samples, especially with M2 fiber webs that have dense fiber density. Therefore the hydrophobicity to the water or ethanol seems to have the relationship of some complicated fiber morphology related properties. To analyze the hydrophobicity on the effects of fiber morphology and topography etc, we have studied the surface properties of the electrospun fiber webs, which forces coming publication. Eventually, the hydrophobicity shows different results according to the surface property of electrospun fiber webs.

3.4. Protection performance

To prepare the sample webs for the protecting test, the electrospun fibers were spun on the PP non-woven substrate until the spun fiber webs were weighted to around 0.0085 g/cm^2 from both methods of solution (S2) and melt (M3), respectively. As depicted in Fig. 10, the pore size of PP non-woven substrate webs was considerably larger than the ones covered with PP electrospun fibers. The substrate webs covered with solution spun fibers showed smaller pore size than the one with melt spun fibers mainly due to smaller fiber diameter. The results of air permeability and water vapor transmission rate are presented in Table 4. It is observed that the PP non-woven webs covered by the electrospun fibers reduced the air permeability up to around 150, which was much higher than most protective clothing materials currently in use (100 $cm^3/s/cm^2$) [4]. However, the air permeability difference between the substrate webs covered by electrospun fibers from solution and from melt was not significant even though there was a big deviation of fiber diameter between two systems. The reduction in water vapor transmission due to electrospun PP fibers found to be insignificant and the resulting water vapor transmission was comparable to those of typical woven work clothing from a reference [4].

The percentage of liquid repellency and penetration measured by two pesticide mixture solutions are also shown in Table 4. A large difference was observed in penetration behavior between two solutions. With the mixture solution (P1) with high surface tension, the repellency was higher than the mixture solution P2, which well corresponds with the trends of contact angle results. In case of bare PP non-woven webs, the repellency was substantially lower and penetration was significantly higher than PP non-woven webs covered by electrospun PP fibers. As shown in Fig. 9, the contact angle of non-woven webs dropped to zero using a droplet of water/ethanol (80/20), while that of electropun PP webs remained high. As a result, the difference in protection performance between bare PP non-woven webs and PP non-woven webs with electrospun PP fibers was much greater for the mixture solution P2 with low surface tension.

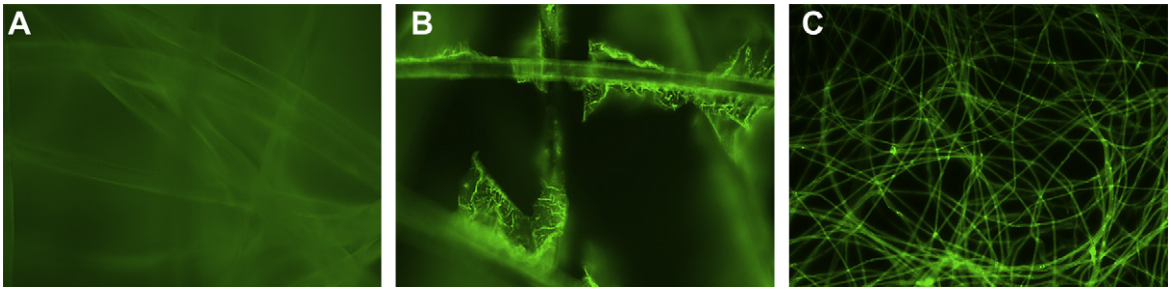

Fig. 11. Protein adsorption results of PP non-woven webs (A), M3 electrospun fiber webs (B), and C2 electrospun fiber webs (C) using BSA labeled with fluorescein isothiocyanate (BSA-FITC).

Although both repellency and penetration are essential in protective coating, the retention of chemicals on the protective material is another important factor. To examine the retention of chemicals on the electrospun fibers, the protein adsorption tests were performed on the fiber surface. As depicted in Fig. 11, a visible increase in fluorescence intensity was observed when electrospun PP fibers laid on PP non-woven webs. The enhanced adsorption of BSA protein by electrospun PP fibers implies that the retention of chemicals can increase by the addition of electrospun PP fibers. A study on the effect of enhanced adsorption on the anti-bacterial activity is currently underway. These results of protection performance and protein adsorption suggest that electrospun PP webs can offer excellent protection without losing permeability in protective clothing applications.

4. Conclusion

We have demonstrated that PP fibers with a diameter ranging from sub-micron meter to 10 μm can be electrospun both from solution at elevated temperature and from melt using the molten polymers. This study reveals that there is only a narrow operational window available (from 140 °C to 170 °C) to electrospin PP fibers from the solution. In the structural studies of PP fibers from the solution, the as-spun PP fibers exhibit the meta-stable β crystal phase which is mainly caused by the elongational deformation of the solution jet and it is confirmed by comparing the β content in two fibers with different sizes. It is also observed that higher collecting temperature not only increases the overall crystallinity of final fibers but also promotes the formation of β crystals. The fibers from the melt exhibit the similar trend but a less degree. The viscosity, solidification as well as deformation appear to influence the induction of β crystals. Finally, all electrospun PP fiber webs from melt and solution (sub-micron to 10 μm) present superior hydrophobicity than PP film, while a commercial PP non-woven web via a film blown process which have thicker diameter (~15 μm) and higher porosity than the electrospun fiber webs show very low contact angle than the film. The PP non-woven webs covered with PP electrospun fiber webs from solution and melt exhibited an outstanding barrier performance and a practical range of air permeability and water vapor transmission in use. In addition to protecting clothing, electrospun PP fibers may be applicable to various other applications such as battery separators due to their large surface area to volume ratio and fine pores constructed from fibers.

References

[1] Noumowe A. Cement and Concrete Research 2005;35(11):2192–8.
[2] Kim J, Hinestroza JP, Jasper W, Barker RL. Textile Research Journal 2009;79 (4):343–50.
[3] Lee S, Obendorf SK. Journal of the Textile Institute 2007;98(2):87–97.
[4] Lee S, Obendorf SK. Journal of Applied Polymer Science 2006;102 (4):3430–7.
[5] Doshi J, Reneker DH. Journal of Electrostatics 1995;35(2&3):151–60.
[6] Dzenis Y. Science (New York, N.Y.) 2004;304(5679):1917–9.
[7] Fridrikh SV, Yu JH, Brenner MP, Rutledge GC. Physical Review Letters 2003;90 (14). 144502/144501–144502/144504.
[8] Hohman MM, Shin M, Rutledge G, Brenner MP. Physics of Fluids 2001;13 (8):2201–20.
[9] Huang Z-M, Zhang YZ, Kotaki M, Ramakrishna S. Composites Science and Technology 2003;63(15):2223–53.
[10] Jun Z, Hou H, Schaper A, Wendorff JH, Greiner A. E-Polymers; 2003. No pp given, Paper No 9.
[11] Reneker DH, Chun I. Nanotechnology 1996;7(3):216–23.
[12] Shin YM, Hohman MM, Brenner MP, Rutledge GC. Applied Physics Letters 2001;78(8):1149–51.
[13] Sukigara S, Gandhi M, Ayutsede J, Micklus M, Ko F. Polymer 2003;44 (19):5721–7.
[14] Larrondo L, St. John Manley R. Journal of Polymer Science Polymer Physics Edition 1981;19(6):909–20.
[15] Larrondo L, St. John Manley R. Journal of Polymer Science Polymer Physics Edition 1981;19(6):921–32.
[16] Larrondo L, St. John Manley R. Journal of Polymer Science Polymer Physics Edition 1981;19(6):933–40.
[17] Lyons J, Li C, Ko F. Polymer 2004;45(22):7597–603.
[18] Lyons JM. Melt-electrospinning of thermoplastic polymers: an experimental and theoretical analysis 2004. p. 196.
[19] Zhou H, Green TB, Joo YL. Polymer 2006;47(21):7497–505.
[20] Zhmayev E, Cho DH, Joo YL. Polymer 2010;51(1):274–90.
[21] Acatay K, Simsek E, Ow-Yang C, Menceloglu Yusuf Z. Angewandte Chemie (International ed. in English) 2004;43(39):5210–3.
[22] Ma M, Hill RM, Lowery JL, Fridrikh SV, Rutledge GC. Langmuir 2005;21 (12):5549–54.
[23] Singh A, Steely L, Allcock HR. Langmuir 2005;21(25):11604–7.
[24] Carroll CP, Joo YL. Physics of Fluids 2006;18(5). 053102/053101–053102/053114.
[25] Wenzel RN. Journal of Industrial and Engineering Chemistry 1936;28:988–94 (Washington, D. C.).
[26] Karger-Kocsis J, Mouzakis DE, Ehrenstein GW, Varga J. Journal of Applied Polymer Science 1999;73(7):1205–14.
[27] Ma M, Mao Y, Gupta M, Gleason KK, Rutledge GC. Macromolecules 2005;38 (23):9742–8.
[28] Dersch R, Liu T, Schaper AK, Greiner A, Wendorff JH. Journal of Polymer Science Part A: Polymer Chemistry 2003;41(4):545–53.
[29] Zhu X, Yan D, Tan S, Wang T, Yan D, Zhou E. Journal of Applied Polymer Science 2000;77(1):163–70.
[30] Torre J, Cortazar M, Gomez M, Ellis G, Marco C. Journal of Polymer Science Part B: Polymer Physics 2004;42(10):1949–59.
[31] Zhmayev E, Cho DH, and Joo YL. Physics of Fluids, submitted for publication.
[32] Zhmayev E, Cho DH, Joo YL. Polymer 2010;51(18):4140–4.
[33] Cho DH, Zhmayev E, and Joo YL. Macromolecules Submitted for publication.